NANO LETTERS

2008
Vol. 8, No. 9
2935-2939

# Atomic-Resolution Imaging of the Nanoscale Origin of Toughness in Rare-Earth Doped SiC

**Aaron M. Kueck,[†,‡] Do Kyung Kim,[§] Quentin M. Ramasse,[||] L. C. De Jonghe,[†,‡] and R. O. Ritchie*[,†,‡]**

*Materials Sciences Division, and National Center for Electron Microscopy, Lawrence Berkeley National Laboratory, Berkeley, California 94720, Department of Materials Science and Engineering, University of California, Berkeley, California 94720, and Department of Materials Science and Engineering, Korea Advanced Institute of Science and Technology, Daejeon 305-701, Korea*

*Received June 20, 2008; Revised Manuscript Received July 29, 2008*

## ABSTRACT

**Ultrahigh-resolution transmission electron microscopy and atomic-scale spectroscopy are used to investigate the origin of the toughness in rare-earth doped silicon carbide (RE-SiC) by examining the mechanistic nature of the intergranular cracking events which we find to occur precisely along the RE-decorated interface between the SiC grains and the nanoscale grain-boundary phase. We conclude that, for optimal toughness, the relative elastic modulus across the grain-boundary phase and the interfacial fracture toughness are the most critical material parameters; both can be altered with judicious choice of rare-earth elements.**

In brittle materials, fracture toughness is invariably the limiting material property for structural applications; it determines the largest flaw that can be tolerated, which impacts everything from material processing requirements (surface finish, porosity) to strength/fracture loads and fatigue lifetimes.[1] Recent suggestions for improving the toughness of ceramic materials include controlling residual stresses, for example, in glass[2,3] and alumina,[4] forming nanocomposites, for example, with carbon nanotubes[5,6] and nanoceramics,[7] or using nature-inspired processing.[8,9] However, the use of sintering additives to create nanometer-scale grain-boundary films or phases has traditionally been the most potent means to develop enhanced toughness in structural ceramics, the objective being to promote intergranular fracture and hence crack deflection and significant crack bridging in the crack wake.

Silicon carbides are potential candidate materials for many ultrahigh-temperature structural applications. For example, using SiC to replace metallic alloys, such as Ni-based superalloys, Ti-6Al-4V, or high-strength steels, in gas-turbine engines for power generation and aerospace applications would permit increases in operating temperatures by many hundreds of degrees, with a consequent dramatic increase in thermodynamic efficiency and reduced fuel consumption; however, to date the use of such ceramic materials has been severely limited by their questionable toughness. In light of this, in situ microstructural toughening techniques have been widely attempted to increase the fracture toughness of SiC; using various sintering additives (dopants), the prime objective has been to induce intergranular fracture in order to develop bridging zones in the crack wake from interlocking grains.[10−13] Intergranular fracture is the essential ingredient here; with a transgranular crack path, no crack bridging can occur with the result that the ceramic has minimal toughness. In addition to the type of dopant, with rare-earth (RE) elements, the presence or absence of intergranular fracture is also related to ionic size.[14] Mechanistically, toughening in liquid-phase-sintered (LPS) materials can be influenced by the mismatch of physical and elastic properties, such as coefficients of thermal expansion (CTE)[15−17] and elastic constants,[18,19] between the grain and the grain-boundary phases, which are typically ∼1 nm in width. In $Al_2O_3$ and $Si_3N_4$, CTE mismatch is a source of significant residual stresses, which can lead to enhanced crack deflection and higher toughness. For SiC, conversely, residual stresses are less of a factor as the CTEs of the grains ($\sim 4.5 \times 10^{-6}$ $°C^{-1}$) and boundary phase ($\sim 3-5 \times 10^{-6}$ $°C^{-1}$)[14] are more comparable. Consequently, toughening is more affected by

* Corresponding author. E-mail: RORitchie@lbl.gov.
† Materials Sciences Division, Lawrence Berkeley National Laboratory.
‡ University of California.
§ Korea Advanced Institute of Science and Technology.
|| National Center for Electron Microscopy, Lawrence Berkeley National Laboratory.

10.1021/nl8017884 CCC: $40.75 © 2008 American Chemical Society
**Published on Web 08/15/2008**

the difference in elastic stiffness between the grain and the boundary phase. In situ toughened SiC is therefore an ideal model system for studying the direct role of a nanoscale property, namely, the elastic modulus of the grain-boundary phase, on macroscopic properties such as fracture toughness.

To understand the mechanistic processes that induce intergranular fracture in SiC, it is necessary for any crack impinging on a grain boundary not to penetrate that boundary but rather to deflect along the boundary itself. On the basis of crack-deflection mechanics for cracks traversing between elastically dissimilar materials,[18] this would require that intergranular cracks in LPS-SiC ceramics propagate along the grain/boundary-phase interface and not within the phase itself. Although it is the essential precursor to developing any degree of useful toughness in SiC, this critical event has never been experimentally proven. Accordingly, we employ ultrahigh resolution imaging here to reveal the precise, atomistic-scale, nature of the intergranular crack trajectories in SiC with respect to the nanoscale boundary films, using rare-earth additives that segregate to the boundary films[20,21] to decorate the interfaces.

Studies were performed on SiC ceramics that were processed with 0.7−1 atom % Y and Yb, as acetate or nitrate salts; the salts were dissolved in methanol and added to submicrometer $\beta$-SiC powder (Betarundum, grade Ultrafine, IBIDEN, Japan), with a mean particle size of 0.27 $\mu$m, 3 wt % Al metal, 0.6 wt % B, and 6 wt % carbon source. The Al powder (H-3, Valimet, Stockton, CA) had an average size of 3 $\mu$m; the boron powder (Alfa Aesar) had a particle size of less than 5 $\mu$m. The carbon was added as polyvinyl-butyral, which yielded ~33% C by weight upon pyrolysis. The powder slurry was ultrasonically agitated, stir-dried, and sieved through a 200 mesh screen. Discs of 38 mm diameter were preformed at room temperature in a steel die, then hot-pressed in a graphite die. Hot pressing was conducted at 1900 °C with 50 MPa applied pressure under flowing argon at 1 atm, with heating and cooling rates of 10 °C/min.

Hot-pressed rounds were ground to remove ~0.5 mm from each surface. Transmission electron microscopy (TEM) foils were then prepared from material at least 1 mm from the edge of the specimen. Stable cracks were produced to study the influence of the nanoscale grain-boundary phases on fracture. Cracks in the TEM foils were introduced via indentation, which was performed before final milling on a 200 $\mu$m thick section; an array of 10 × 10 microindents (50 g load with a cube-corner indenter) was produced on a polished surface. Mechanical thinning and ion milling proceeded from the opposite side to preserve the cracks. Indentation after final milling utilized five indentations, made using a nanoindenter with a corner-cube indenter (under 6000 $\mu$N normal load), which were placed near the thin edge of the foil to produce cracks which ran toward the thinned region. It was imperative that both crack faces were intact and remained located near each other to allow analysis of mating fracture surfaces. Indentation before or after final foil milling produced identical crack surfaces, indicating that machining and milling during sample preparation had not damaged the crack faces.

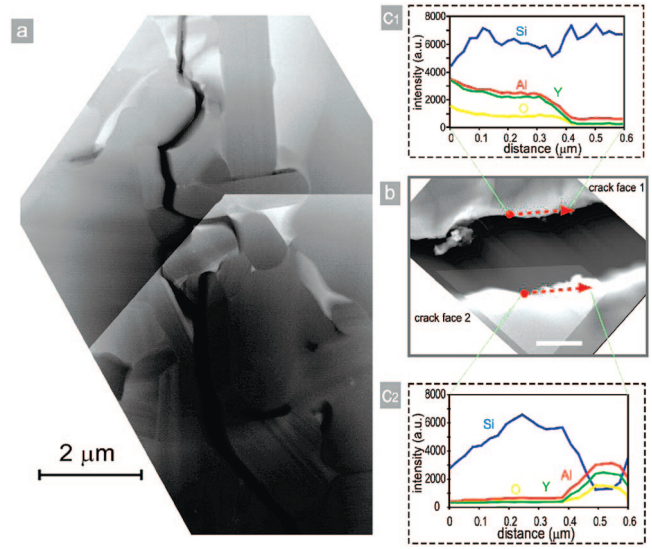


**Figure 1.** (a) Dark field STEM image of an intergranular crack in SiC with Al, B, C, and Y sintering additives. Crack deflection along grain boundaries is readily apparent; the crack appears black in dark field. (b) Dark field STEM image of two opposing crack faces. Lines along the crack faces indicate the position of EDS line scans, performed with a 1 nm probe size (scale is 500 nm). (c1, c2) Integrated EDS intensity vs distance along the line for Si, Al, Y, and O on each crack face (1 and 2). Grain-boundary phase material (highly enriched in Al, Y, and O) is present along exactly one crack face. This indicates that the fracture location is at the interface between the SiC grain and the grain-boundary phase. Also note that the interface along which the crack propagates switches from crack face 1 (top) to crack face 2 (bottom) near the end of the scan. This could correspond to a change in the direction of the crack.

Elemental mapping using electron energy loss spectroscopy (EELS) and nanoprobe energy dispersive spectroscopy (EDS) was conducted using a Philips CM200/FEG TEM. Mapping was performed using a post-edge energy-filtered image and background subtraction using two pre-edge images. EDS was carried out in STEM mode with a 1 nm spot size. Signals were integrated over the peak width using the Si, Al, and O K-lines and either the RE K- or L-lines. High-resolution high-angle annular dark field (HAADF) images and EELS were performed using a VG HB501 dedicated STEM with a spot size of 1 Å (imaging) or 1.5 Å (spectroscopy). Semiconvergence angles were 20 mrad (imaging) and 28 mrad (spectroscopy). The HAADF collection angle range was 74−215 mrad; the EELS collection angle was 12 mrad, and the resolution was 0.1 eV. Spectroscopic methods were used to determine the relative location of the crack paths with respect to the SiC grains and the nanometer-wide grain-boundary phases.

EDS line scans of opposing crack faces (Figure 1) and elemental mapping with EELS (Figure 2) both demonstrated that the intergranular cracks formed along the nanometer-wide grain-boundary phase (GBP). Segregation of Al, O, and RE could be clearly identified in this phase, with the cracks located strictly along one side of the boundary phase. Figure 1c highlights the contrast between the compositions of the two crack faces. While one fracture surface exhibits Al, Y,

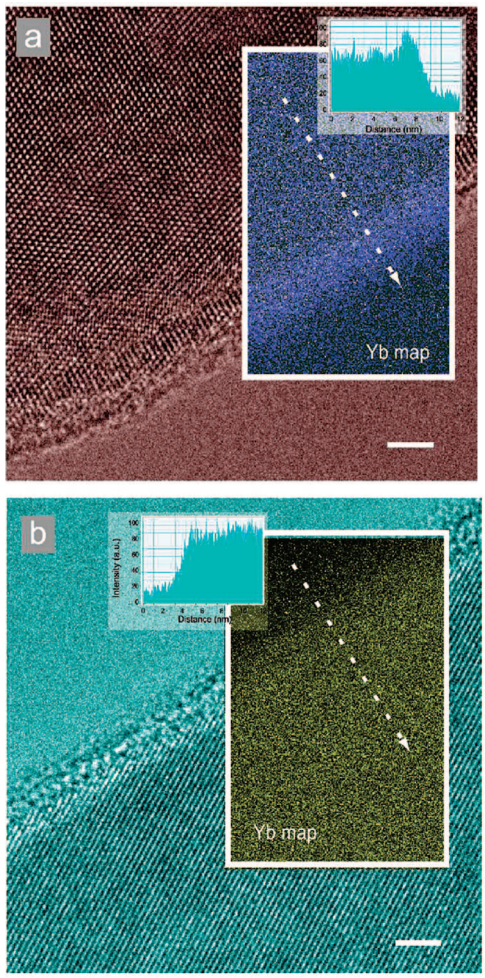


**Figure 2.** (a) Bright field HRTEM and Yb elemental map (overlay) of an intergranular crack face in SiC with Al, B, C, and Yb additives (scale is 2 nm). The Yb map shows a dramatic increase in the Yb signal along the edge of the crack (see intensity profile inset), indicating the presence of the grain-boundary phase. Nanoprobe EDS at the edge confirms enrichment of Yb, Al, and O. (b) Bright field HRTEM and Yb elemental map (overlay) of the intergranular crack face opposite that in Figure 2a. The Yb map shows no contrast (see intensity profile inset), indicating the lack of Yb along this crack face. Nanoprobe EDS at the edge finds (1) bulk value of Al, (2) lack of Yb, and (3) slight enrichment of O. This indicates that the crack propagates precisely along the interface between the SiC grain and the RE-bearing grain-boundary phase, as is seen in the material with Y (Figure 1).

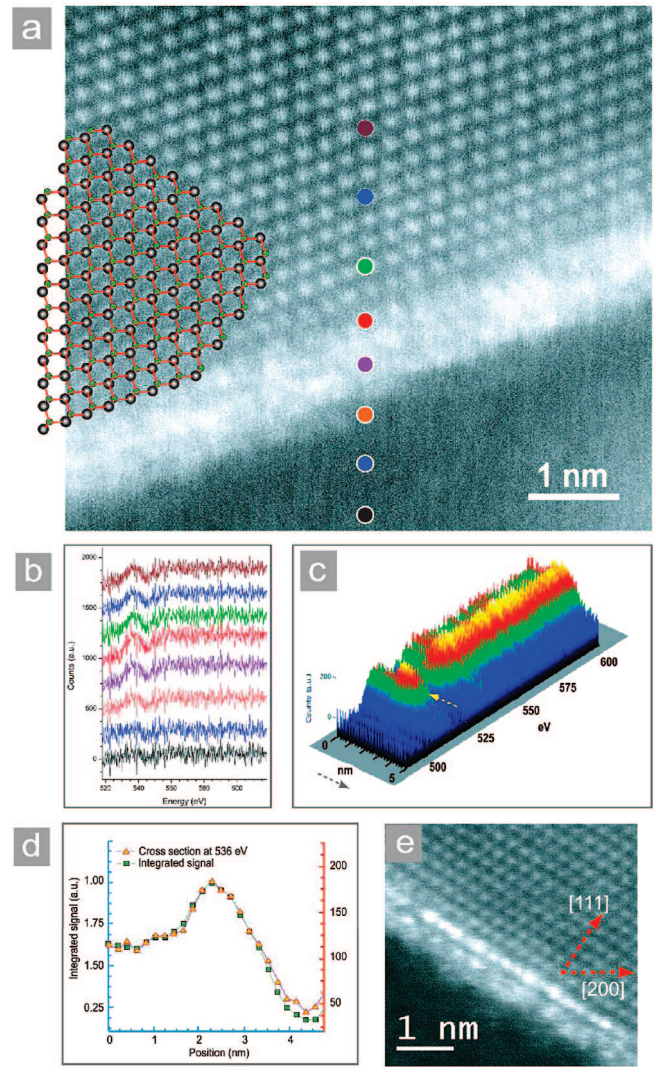


**Figure 3.** (a) Z-contrast image of a grain boundary. Bright contrast in the grain-boundary phase indicates enrichment of Yb. (b) O K-edge EELS scans along the line indicated in Figure 3a. O peak height is greatest within the grain-boundary phase. (c) 3-D plot of the EELS scans along the line in Figure 3a. The O peak is indicated with an arrow. The O chemical width of the boundary is ~2 nm; this is twice the Yb chemical width from the Z-contrast image. Crack propagation occurs along the interface determined by the enrichment of RE, not the interface determined by O. This is a sensible result as RE-C(O) bonds should be weaker than Si−C(O) bonds; the RE-containing interface is the weakest plane and most likely to fracture. (d) O peak height at 536 eV and total O peak integrated intensity from 528 to 624 eV vs distance along the scan. The chemical width of the grain-boundary phase is ~1.4 nm, and there is an area of O enrichment ~1 nm in width in the aligned grain (upper portion of 3a). (e) Yb-enriched grain boundary which has been aligned with the beam to show the location of the RE columns. Yb-containing columns terminate each plane of the SiC lattice, aligning along the [200] direction.

and O signals that approach or exceed Si, the opposite surface contains only background counts of the GBP constituents. Figure 2 shows this contrast visually; the bright edge along one fracture surface reveals the Yb present only in the boundary phase. Indeed, all intergranular cracks in both Y- and Yb-containing materials showed identical behavior with the intergranular crack following an exact path along one side of the boundary phase.

The side of the crack not adjacent to grain-boundary material was chemically indistinguishable from the center of a SiC grain. The crack surface on this side was slightly enriched with oxygen (O), although high-spatial-resolution EELS suggested that minimal O enrichment is a characteristic of the SiC lattice near grain boundaries. Figure 3 shows that the O peak height near a grain boundary is increased ~1 nm into the SiC grain, well beyond the extent of the GBP. Indeed, enrichment of O near grain boundaries has been predicted in silicon nitride, which has similar grain-boundary phases.[22,23] Our analysis of numerous similar foils confirmed that this specific location of the fracture was definitively between the RE-containing grain-boundary phase and the

O-enriched SiC lattice, which strongly implies that the interface defined by RE segregation is the most relevant for fracture. This points to the plane containing RE-C(O) bonds as the weakest link, making this interface the most likely to fracture.

Figure 3e shows a Yb-enriched grain boundary which has been aligned with the beam to show the location of RE-containing columns along the interface. Bright columns, indicating the presence of RE atoms, can be seen to terminate each SiC plane along the [200] direction. Unlike $Si_3N_4$, which often exhibits two possible RE locations along the interface,[21,22] the GBP in SiC has only one interfacial RE location. This coincides with the difference in the structure of the ceramic surfaces. $Si_3N_4$ interfaces consist of open rings, leading to two possible attachment locations, whereas SiC interfaces are atomically flatter, presenting only one possible attachment location for the large RE atoms.

This result, that any crack impinging on the grain-boundary phase will not penetrate the phase but rather "delaminate" along the boundary-phase/SiC interface, is entirely consistent with linear-elastic crack deflection mechanics, specifically the He and Hutchinson solution[18] for predicting whether a crack penetrates or arrests/delaminates at a dissimilar material interface. The important parameters in this model are (i) the incident angle, which is microstructure-dependent, (ii) the modulus mismatch across the interface $(E'_{SiC} - E'_{GBP})/(E'_{SiC} + E'_{GBP})$, that is, the relative elastic modulus of the boundary phase, which is chemistry- and structure-dependent ($E'_{SiC}$ and $E'_{GBP}$ are, respectively, the Young's moduli of the SiC grain and boundary phase), and (iii) the relative fracture toughness of the interface $G_{interface}$ (which depends on the interface bonding) and that of the boundary phase $G_{GBP}$. Rare-earth additives can alter both the stiffness of the boundary phase and the toughness of the interface.

Figure 4 presents the He and Hutchinson solution for SiC/GBP with a crack at an interface incident at 90°, showing a plot of the relative interfacial toughness versus the relative elastic modulus along with a bounding line between interface penetration or deflection (interface delamination). Normal incidence along the boundary represents the geometrically worst-case scenario; a shallower angle increases the likelihood for crack deflection. Included are images of cracks in RE-doped SiC at near 90° incidence. The observation of both crack penetration and deflection suggests that the RE-SiC system is near the bounding line between these two types of cracking behavior and is therefore very sensitive to the choice of rare-earth dopant. This presents the opportunity to estimate the relative interfacial toughness in our system, if the elastic properties of the boundary phase are known.

Possible values for the elastic modulus of the GBP vary. Oxynitride glasses have low elastic moduli, with $E \sim 150$ GPa.[24] Crystalline $Al_2OC$, a second phase material commonly seen in ABC-SiC and a possible GBP, has a much higher $E$ of 225 GPa.[25] An intermediate modulus of 209 GPa has been calculated for the GBP of $Si_3N_4$ with Y.[26] Using this latter value of $E$ for the GBP, we can estimate the relative interfacial toughness in our material as 0.4 times the toughness of the GBP.

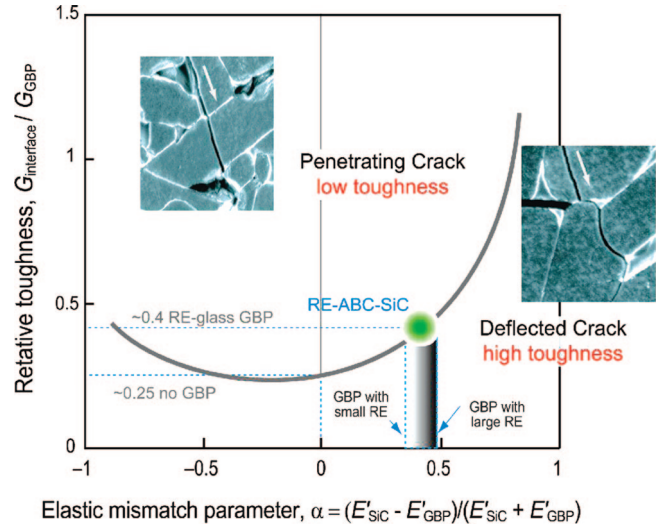


**Figure 4.** He and Hutchinson's solution for a crack impinging an interface between two elastically dissimilar materials at 90°. The curve marks the boundary between systems in which cracks are likely to penetrate the interface (above the curve) or deflect along the interface (below the curve). Experimental trends in RE-doped SiC show a transition from crack deflection to interface penetration as the radius of the RE ion decreases, suggesting that these systems lie near the bounding curve. Shown are likely values for the elastic mismatch, based on calculated elastic modulus values for the boundary phase ($E_{GBP}$).[26] The interfacial toughness is then ~0.4 times the toughness of the grain-boundary phase. Small deviations in interfacial toughness, driven by changes in the ionic size of the RE additives along the interface, can push the crack to deflect along the boundary (large RE), resulting in intergranular fracture and high toughness, or penetrate the boundary (small RE), resulting in transgranular fracture and minimal toughness.

On the basis of bulk glass measurements and simulations of the properties of the grain-boundary phases, it is expected that the addition of RE will increase the modulus of the grain-boundary phase,[26,27] with smaller ions having the larger effect. With a larger $E'_{GBP}$ associated with the addition of RE ions, the elastic mismatch between SiC and the boundary phase will be progressively decreased, which from Figure 3 will reduce the likelihood of crack deflection along, rather than through, the interface. This implies that the addition of smaller RE ions to SiC should diminish the probability of intergranular fracture and hence degrade the toughness, as has been seen experimentally.[14,28,29]

RE additives should also affect the toughness of the interface. RE ions can act as network modifiers in glassy-boundary phases; high-coordination, large radius RE ions should lower the local strength of the glass.[30] Replacing a Si or Al atom along the interface with a RE ion would be expected to lower the toughness of the interface;[31,32] accordingly, large RE ions will certainly have the greatest effect. The largest decrease in interfacial toughness in the presence of large RE ions, combined with a lower elastic modulus of the boundary phase, makes crack deflection at, and then "delamination" along, the interface more likely; this confirms that doping with large RE ions will promote intergranular fracture and hence enhance the toughness of the ceramic, again consistent with experiments.[14,28,29]

In conclusion, nanoscale-resolution microscopy and spectroscopy has demonstrated that intergranular cracks in SiC with rare-earth additives propagate precisely along the interface between the SiC grains and the nanometer-wide RE-containing grain-boundary phase. This fracture behavior can be understood in terms of the He and Hutchinson model for the interaction of elastic cracks with interfaces. Crack deflection along the interface in these materials can be altered by choice of rare-earth elements; larger ions enhance the likelihood of intergranular fracture and consequently increase the toughness, providing a striking example of the direct link across some eight orders of dimensions between nanoscale events and the macroscopic mechanical properties of materials.

**Acknowledgment.** This work was supported by the Director, Office of Science, Office of Basic Energy Sciences, Materials Sciences and Engineering Division, of the U.S. Department of Energy under Contract No. DE-AC02-05CH11231. Part of this work was carried out using the facilities at the National Center for Electron Microscopy, which is supported at the Lawrence Berkeley National Laboratory by the Department of Energy under the same contract number. D.K.K. would like to thank the SBS Foundation and Korea Research Foundation (KRF-2005-005-J09701) for supporting his sabbatical leave in Berkeley where the study was performed.

## References

(1) Clegg, W. J. *Science* **1999**, *286*, 1097–1099.
(2) Green, D. J.; Tandon, R.; Sglavo, V. M. *Science* **1999**, *283*, 1295–1297.
(3) Zhang, Y.; Wang, W. H.; Greer, A. L. *Nat. Mater.* **2006**, *5*, 857–860.
(4) Rao, M. P.; Sanchez-Herencia, A. J.; Beltz, G. E.; McMeeking, R. M.; Lange, F. F. *Science* **1999**, *286*, 102–105.
(5) Zhan, G.-D.; Kuntz, J. D.; Wan, J.; Mukherjee, A. K. *Nat. Mater.* **2002**, *2*, 38–42.
(6) Peigney, A. *Nat. Mater.* **2002**, *2*, 15–16.
(7) Zhang, X. F.; Harley, G.; De Jonghe, L. C. *Nano Lett.* **2005**, *5*, 1035–1037.
(8) Deville, S.; Saiz, E.; Nalla, R. K.; Tomsia, A. P. *Science* **2006**, *311*, 515–518.
(9) Ahn, E. S.; Gleason, N. J.; Nakahira, A.; Ying, J. Y. *Nano Lett.* **2001**, *1*, 149–153.
(10) Cao, J. J.; MoberlyChan, W. J.; De Jonghe, L. C.; Gilbert, C. J.; Ritchie, R. O. *J. Am. Ceram. Soc.* **1996**, *79*, 461–469.
(11) Zhang, X.-F.; Yang, Q.; De Jonghe, L. C. *Acta Mater.* **2003**, *51*, 3849–3860.
(12) Lee, S.; Kim, Y.; Mitomo, M. *J. Am. Ceram. Soc.* **2001**, *84*, 1347–1353.
(13) Strecker, K.; Ribeiro, S.; Oberacker, R.; Hoffmann, M.-J. *Int. J. Refract. Metals Hard Mat.* **2004**, *22*, 169–175.
(14) Zhou, Y.; Hirao, K.; Toriyama, M.; Yamauchi, Y.; Kanzaki, S. *J. Am. Ceram. Soc.* **2001**, *84*, 1642–1644.
(15) Hsueh, C.-H.; Becher, P. F. *Mater. Sci. Eng., A* **1996**, *212*, 22–28.
(16) Li, Z.; Bradt, R. C. *J. Am. Ceram. Soc.* **1989**, *72*, 70–77.
(17) Peterson, I. M.; Tien, T.-Y. *J. Am. Ceram. Soc.* **1995**, *78*, 2345–2352.
(18) He, M.-Y.; Hutchinson, J. W. *Int. J. Solids Structures* **1989**, *25*, 1053–1067.
(19) McNaney, J. M.; Cannon, R. M.; Ritchie, R. O. *Int. J. Fract.* **1994**, *66*, 227–240.
(20) Ziegler, A.; Idrobo, J. C.; Cinibulk, M. K.; Kisielowski, C.; Browning, N. D.; Ritchie, R. O. *Science* **2004**, *306*, 1768–1770.
(21) Dwyer, C.; et al. *J. Mater. Sci.* **2006**, *41*, 4405–4412.
(22) Bishop, C. M.; Cannon, R. M.; Carter, W. C. *Acta Mater.* **2005**, *53*, 4755–4764.
(23) Hudson, T. S.; Nguyen-Mahn, D.; van Duin, A. C. T.; Sutton, A. P. *Mater. Sci. Eng., A* **2006**, *422*, 123–135.
(24) Becher, P. F.; et al. *Acta Mater.* **1996**, *44*, 3881–3893.
(25) Yu, R.; Zhang, X.-F.; De Jonghe, L. C.; Ritchie, R. O. *Phys. Rev. B* **2007**, *75*, 104114.
(26) Chen, J.; Ouyang, L.; Rulis, P.; Misra, A.; Ching, W. Y. *Phys. Rev. Lett.* **2005**, *95*, 256103.
(27) Hampshire, S.; Pomeroy, M. J. *J. Non-Cryst. Solids* **2004**, *344*, 1–7.
(28) Satet, R. L.; Hoffmann, M. J.; Cannon, R. M. *Mater. Sci. Eng., A* **2006**, *422*, 66–76.
(29) Liu, Q.; Gao, L.; Yan, D. S.; Thompson, D. P. *Mater. Sci. Eng., A* **1999**, *269*, 1–7.
(30) Marchi, J.; Morais, D. S.; Schneider, J.; Bressiani, J. C.; Bressiani, A. H. A. *J. Non-Cryst. Solids* **2005**, *351*, 863–868.
(31) Nakayasu, T.; Yamada, T.; Tanaka, I.; Adachi, H.; Goto, S. *J. Am. Ceram. Soc.* **1998**, *81*, 565–570.
(32) Sun, E. Y.; Alexander, K. B.; Becher, P. F.; Hwang, S.-L. *J. Am. Ceram. Soc.* **1996**, *79*, 2626–2632.

NL8017884